Copper-Plumbagin Complex Produces Potent Anticancer Effects by Depolymerizing Microtubules and Inducing Reactive Oxygen Species and DNA Damage

Sandipan Mukherjee,[§] Avishkar V. Sawant,[§] Shweta S. Prassanawar, and Dulal Panda*

Read Online

ACCESS | Metrics & More | Article Recommendations | SI Supporting Information

ABSTRACT: Here, we have synthesized a copper complex of plumbagin (Cu-PLN) and investigated its antiproliferative activities in different cancer cells. The crystal structure of Cu-PLN showed that the complex was square planar with a binding stoichiometry of 1:2 (Cu/Plumbagin). Cu-PLN inhibited the proliferation of human cervical carcinoma (HeLa), human breast cancer (MCF-7), and murine melanoma (B16F10) cells with half-maximal inhibitory concentrations (IC50) of 0.85 ± 0.05, 2.3 ± 0.1, and 1.1 ± 0.1 μM, respectively. Plumbagin inhibited the proliferation of HeLa, MCF-7, and B16F10 cells with IC50 of 7 ± 0.1, 8.2 ± 0.2, and 6.2 ± 0.4 μM, respectively, showing that Cu-PLN is a stronger antiproliferative agent than plumbagin. Interestingly, Cu-PLN showed much stronger toxicity against breast carcinoma and skin melanoma cells than noncancerous breast epithelial and skin fibroblast cells, indicating its specific cytotoxicity toward cancer cells. A short exposure of Cu-PLN triggered microtubule disassembly in cultured cancer cells, and the complex also inhibited the polymerization of purified tubulin much more strongly than plumbagin. Furthermore, Cu-PLN inhibited the binding of colchicine to tubulin. In addition to microtubule depolymerization, the antiproliferative mechanism of Cu-PLN involved induction of reactive oxygen species, reduction of the mitochondrial membrane potential, and DNA damage. Moreover, the cytotoxic effects of Cu-PLN reduced significantly in cells pre-treated with *N*-acetyl cysteine, suggesting that reactive oxygen species generation is crucial in Cu-PLN's mode of action. Thus, the complexation of plumbagin with copper yields a promising antitumor agent having a stronger antiproliferative activity than cisplatin, a widely used anticancer drug.
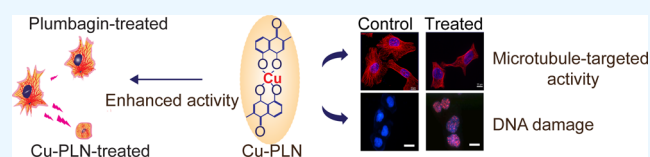
INTRODUCTION

Metal complexes exhibit enhanced therapeutic potential than free drugs; when complexed with metals, many compounds show increased cytotoxicity and an improved pharmacokinetic profile.[1,2] Thus, developing novel metallodrugs has become an exciting area of medicinal chemistry. The generation of metal complexes has also attracted an immense interest in cancer chemotherapy owing to the different three-dimensional geometries of the metal complexes, the possibility of intracellular redox reactions, and the targeting of DNA and critical intracellular proteins.[1,3] Platinum-containing metal complexes such as cisplatin, carboplatin, and oxaliplatin have been extensively studied for their anticancer properties and used for treating various tumors.[4] However, the clinical use of these drugs is limited due to dose-related toxicity issues and acquired resistance by cancer cells.[5] Alternative metal complexes containing ions such as copper, zinc, gold, and ruthenium have received significant interest.[6,7] Among these, copper-based complexes have gained wide traction for their therapeutic potential as antitumor agents.[8,9]

The development of copper-based antineoplastic agents stems from the hypothesis that copper is an endogenous metal, and its concentration in the human body is tightly regulated. Furthermore, altered metabolism in cancerous cells leads to a higher accumulation of copper than in noncancerous cells.[10,11] Hence, copper-based metal complexes are anticipated to accumulate in higher concentrations inside cancer cells, thus causing selective and increased cytotoxicity in cancer cells. Copper complexes also have higher lipophilicity, enabling higher accumulation and a concomitant increase in anticancer activity.[9] Complexation of ligands with copper reduces the half-maximal inhibitory concentration (IC$_{50}$) of ligands by several folds, implying enhanced potency.[9] For example, the IC$_{50}$ of 8-hydroxyquinoline-based ligand in HeLa cells decreased by 13-fold when complexed with copper.[12] Furthermore, a square planar copper-plumbagin metal complex displayed enhanced cytotoxicity against different cancer cells.[13]

Plumbagin is a naturally occurring naphthoquinone known for its anti-inflammatory, anticancer, and antibacterial activities.[14−16] It also displays potent in vivo antitumor activity against cancer cells such as breast, prostate, ovarian, bladder,

glioma, and non-small cell lung cancer.[17] The anticancer mechanism of plumbagin involves a multi-mode approach, which includes disruption of microtubules and various cell-signaling pathways such as NF-kβ, STAT3, and AKT.[17,18] Plumbagin also induces cell cycle arrest, reactive oxygen species (ROS) production, DNA damage, apoptosis, and autophagy.[17] However, there is a limited therapeutic potential of plumbagin due to the lack of cell specificity,[19−21] poor pharmacokinetics, and low lipophilicity resulting in reduced intracellular uptake.[22,23] A copper-plumbagin complex was synthesized to enhance the pharmacokinetic profile and antitumor activity of plumbagin.[13] Because the complex exhibited superior cytotoxicity than plumbagin,[13] we wanted to explore its anticancer activity and elucidate its mechanism of action.

In this study, we synthesized the copper-plumbagin metal complex (Cu-PLN), as reported previously,[13] and characterized the complex using X-ray diffraction analysis, Fourier transform infrared (FTIR), high-resolution mass spectrometry (HRMS), and reverse phase high-pressure liquid chromatography (RP-HPLC). Cu-PLN exerted superior, selective, and sustained antiproliferative activity than plumbagin against various cancer cell lines. In addition, we show that the anticancer activity of Cu-PLN involves disassembling microtubules, ROS generation, and DNA damage. The results suggest that Cu-PLN is a potent antiproliferative agent with promising anticancer activity.

■ RESULTS

Characterization of the Copper-Plumbagin Metal Complex (Cu-PLN). We synthesized the copper-plumbagin complex and elucidated its anticancer mechanism of action. Initially, the molecular descriptors of plumbagin and Cu-PLN were determined (Figure 1). The partition coefficient (log P)
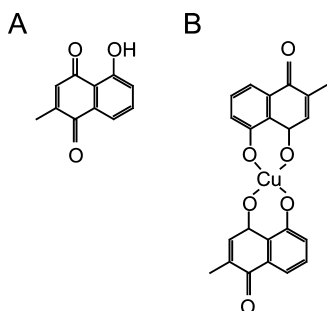
**Figure 1.** Chemical structures of (A) plumbagin and (B) copper-plumbagin metal complex (Cu-PLN).

and topological polar surface area (TPSA) for plumbagin were estimated to be 1.78 and 54.37 Å^2/molecule, respectively. In the case of Cu-PLN, log P and TPSA were 2.79 and 71.08 Å^2/molecule, respectively, indicating that the complex is lipophilic and can be absorbed across transcellular routes.[24,25]

Upon the addition of divalent copper to plumbagin, the absorbance spectra underwent a bathochromic shift, with a decrease in the maxima at 410 nm (A_{410}) and the appearance of a new absorbance maxima at 530 nm (A_{530}) (Figure 2A). There was a dose-dependent increase in the absorbance at A_{530} with the increase in Cu^{2+} concentration, which saturated at 50 μM Cu^{2+} (Figure 2B). Considering the change in absorbance on the addition of Cu^{2+} to plumbagin, the subsequent endeavor was to generate a copper-plumbagin metal complex

(Cu-PLN). To this end, as reported previously, CuCl$_2$ was added to plumbagin and refluxed for 2 h.[13] On evaporation of the solution, dark red crystals of Cu-PLN were obtained. The mass of the generated Cu-PLN was 437.3, which agreed with the anticipated and reported mass of the metal complex (Figure 2C).[13] A single peak in the high-performance liquid chromatography (HPLC) chromatogram for Cu-PLN indicated that the complex was pure, with purity estimated at 96.4% (Figure 2D). The elution time of plumbagin and Cu-PLN was 7.9 and 16.1 min, respectively (Figure 2D). The increase in the retention time of Cu-PLN is possibly due to the higher molecular weight of the complex. Furthermore, FTIR indicated the formation of new bonds in Cu-PLN as new vibrational frequencies were observed at 3431 cm^{-1}, indicating the formation of the O−Cu−O bond in Cu-PLN (Figure 2E). The structure of Cu-PLN was square planar, as reported previously,[13] and the binding stoichiometry was determined to be 1:2 (Cu/Plumbagin) (Figure S1 and Table S1). The Cu−O bond length was estimated to be 1.9 Å (4), and the O−Cu−O bond angle was 92.25 (14)° (Table S1). Subsequently, the antiproliferative activity of the synthesized Cu-PLN complex was determined.

Cu-PLN Strongly Inhibited the Proliferation of Cancer Cells than Noncancerous Cells. Cu-PLN produced more potent cytotoxicity in HeLa, MCF-7, and B16F10 cells than plumbagin (Figure 3A−C). For example, Cu-PLN and plumbagin inhibited HeLa cell proliferation with IC$_{50}$ of 0.85 ± 0.05 and 7 ± 0.1 μM, respectively, indicating that Cu-PLN exerted ~8 times stronger antiproliferative activity than plumbagin (Table 1). In addition, Cu-PLN displayed lower antiproliferative activity against noncancerous cells as compared to cancerous cells (Figure 3D,E and Table 1). IC$_{50}$ of Cu-PLN in MCF-7 cells and its noncancerous counterpart MCF10A cells were 2.3 ± 0.1 and 25 ± 0.8 μM, respectively, showing a 10-fold higher activity against cancerous cells (Table 1). Similarly, Cu-PLN displayed sevenfold higher activity in cancerous B16F10 cells (1.1 ± 0.1 μM) than noncancerous L929 cells (7.4 ± 0.6 μM) (Table 1). Several folds higher antiproliferative activity of Cu-PLN against cancer cells than non-cancer cells indicated the selectivity of Cu-PLN. Interestingly, plumbagin did not display such selectivity as it exhibited similar antiproliferative activity against both cancerous MCF-7 cells (8.2 ± 0.2 μM) and noncancerous MCF10A cells (11.7 ± 0.5 μM) (Table 1). Plumbagin also displayed higher antiproliferative activity against the noncancerous L929 cells than cancerous B16F10 cells (Table 1). The results suggest that Cu-PLN is highly selective in killing cancer cells, while plumbagin does not exhibit such selective cytotoxicity.

Cu-PLN Inhibited the Viability of Cancer Cells over Two Cell Cycles. Next, the effect of plumbagin and Cu-PLN on the viability of HeLa cells was assessed using propidium iodide (PI) staining. At similar concentrations, plumbagin had no significant effect on cell viability, whereas Cu-PLN strongly inhibited cell viability after 24 h treatment (Figure 4). The percentages of PI-positive cells were 5 ± 1.7, 6 ± 1.3 (p > 0.05), and 7 ± 1.8% (p > 0.05) in the presence of vehicle, 1, and 2 μM plumbagin, respectively, suggesting no cell death (Figure 4A−C). However, the number of PI-positive cells significantly increased to 54 ± 13.5 (p < 0.01) and 74 ± 10.9% (p < 0.001) in the presence of 1 and 2 μM Cu-PLN, respectively (Figure 4D−F). The high percentage of PI-positive cells obtained after Cu-PLN treatment indicated that
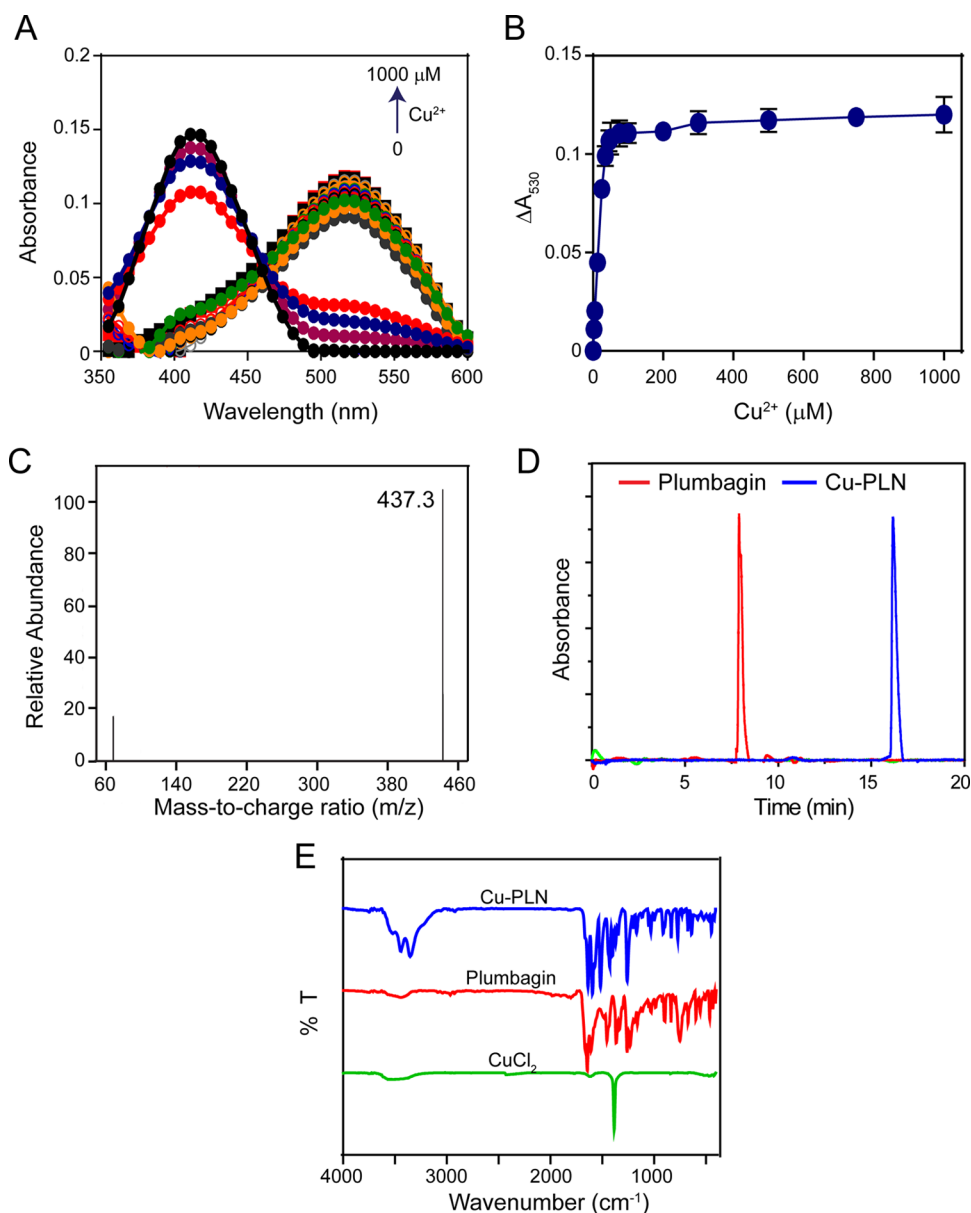
Figure 2. Characterization of Cu-PLN. (A) Absorbance spectra of plumbagin without or with Cu^{2+}. Plumbagin (25 μM) was incubated in the absence or presence of increasing concentrations of $CuCl_2$ (2.5−1000 μM), and then absorbance spectra were recorded. The representative spectra are as follows: 25 μM plumbagin in the absence (●) or the presence of 2.5 (violet ●), 5 (blue ●), 12.5 (red ●), 25 (grey ●), 35 (orange ●), 45 (green ●), 50 (○), 75 (red ○), 100 (blue ○), 200 (green ○), 300 (orange ○), 500 (gray ○), 750 (■), and 1000 (red ■) μM $CuCl_2$. (B) The change in absorbance of plumbagin at 530 nm in the absence or presence of increasing concentrations of Cu^{2+}. Error bars represent standard deviation. (C) Electrospray ionization spectra of Cu-PLN obtained from HRMS-Orbitrap. (D) A representative chromatogram of plumbagin and Cu-PLN. RP-HPLC of plumbagin (red trace) and Cu-PLN (blue trace) was performed in gradient mode, with 0.1% trifluoroacetic acid (TFA) in water and 0.1% TFA in acetonitrile-methanol mixture (green trace). (E) FTIR of $CuCl_2$ (green trace), plumbagin (red trace), and Cu-PLN (blue trace). KBr pellets were made with $CuCl_2$, plumbagin, or Cu-PLN, and FTIR spectra were recorded.

the metal complex caused significantly higher cell death than plumbagin (Figure 4F).

Furthermore, Cu-PLN showed sustained cytotoxicity in different cancer cells (Figure 5). After 48 h of treatment of HeLa cells with the vehicle, 1 μM plumbagin, and 1 μM Cu-PLN, the numbers of PI-positive cells were 11 ± 2.2, 14 ± 2.2 ($p > 0.05$), and 86 ± 6.0% ($p < 0.0001$), respectively (Figure 5A,D). To ascertain whether the sustained anticancer activity of Cu-PLN is not cell line-specific, we checked the effect of Cu-PLN on the viability of B16F10 and MCF-7 cells after two cell cycles (Figure 5B,C). In B16F10 cells, the numbers of PI-positive cells in the presence of vehicle, 1 μM plumbagin, and 1

μM Cu-PLN were 11 ± 0.6, 19 ± 7 ($p > 0.05$), and 98 ± 2% ($p < 0.0001$), respectively (Figure 5B,D). Similarly, in MCF-7 cells, the number of PI-positive cells in the presence of vehicle, 1 μM plumbagin, and 1 μM Cu-PLN was 22.6 ± 1.1, 23 ± 1.5 ($p > 0.05$), and 48 ± 7.7% ($p < 0.001$), respectively (Figure 5C,D). The results indicated that the antiproliferative activity of Cu-PLN can sustain for at least two cell cycles against different cancer cells in culture (Figure 5D).

Cu-PLN Depolymerized Microtubules in HeLa Cells and Inhibited In Vitro Tubulin Assembly. Plumbagin perturbed the microtubule organization in cultured cancer cells.[18] Therefore, we wanted to determine the effect of Cu-
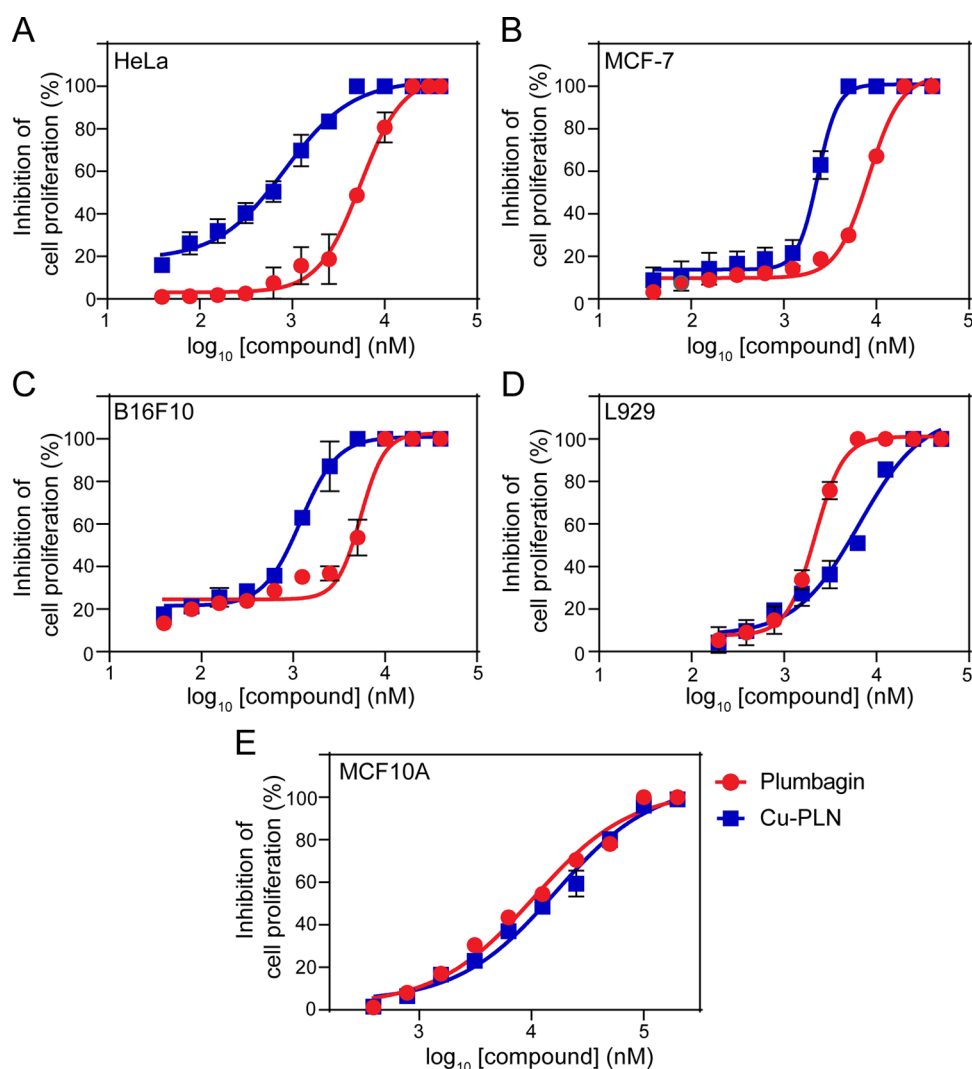
Figure 3. Cu-PLN exhibited enhanced antiproliferative activity than plumbagin. Cells were incubated with different concentrations of plumbagin (red ●) or Cu-PLN (blue ■). The percentage inhibition of cell proliferation was estimated using sulforhodamine B assay. Inhibition of cell proliferation was determined in (A) HeLa, (B) MCF-7, (C) B16F10, (D) L929, and (E) MCF10A cells. The error bars represent the standard deviation.

**Table 1. Antiproliferative Activity of Plumbagin and Cu-PLN**

	IC$_{50}$ (μM)	
cell lines	plumbagin	Cu-PLN
HeLa	7 ± 0.1	0.85 ± 0.05
MCF-7	8.2 ± 0.2	2.3 ± 0.1
MCF10A	11.7 ± 0.5	25 ± 0.8
B16F10	6.2 ± 0.4	1.1 ± 0.1
L929	2.2 ± 0.1	7.4 ± 0.6

PLN on the microtubule network in HeLa cells. Treatment of HeLa cells with 1 and 2 μM Cu-PLN for 2, 4, and 12 h resulted in microtubule depolymerization (Figure 6A). The mean microtubule intensity per cell decreased significantly within 2 h in the presence of 1 ($p < 0.05$) and 2 ($p < 0.01$) μM Cu-PLN compared to the control cells, indicating that even a short exposure of the metal complex can visibly disassemble the microtubule network (Figure 6B). The disassembly of microtubules was even higher after 4 and 12 h Cu-PLN treatment (Figure 6B).

Because Cu-PLN strongly depolymerized microtubules in HeLa cells, we next analyzed the effect of the complex on taxol-induced assembly of purified tubulin. In comparison to plumbagin, Cu-PLN led to a higher inhibition of tubulin assembly (Figure 7A,B). In the presence of 20, 30, 50, and 60 μM plumbagin, the extent of tubulin polymerization was inhibited by 4 ± 1.3, 6 ± 2.4, 13 ± 1.8, and 16 ± 0.3%, respectively (Figure 7C). In contrast, 20, 30, 50, and 60 μM Cu-PLN produced a more pronounced inhibitory effect as it inhibited tubulin polymerization by 18 ± 1.2, 37 ± 1.2, 56 ± 2.2, and 68 ± 2.0%, respectively (Figure 7C). The results suggested that Cu-PLN is a more potent inhibitor of microtubule assembly than plumbagin.

Cu-PLN Bound to Tubulin at the Colchicine-Binding Site. We performed a molecular docking analysis to determine the putative binding site of Cu-PLN on the tubulin heterodimer. Cu-PLN bound at the interface of the $\alpha\beta$-tubulin heterodimer near the colchicine site (Figure 8A−D). Two probable binding modes of Cu-PLN were identified with similar binding energies of −9.8 and −9.7 kcal/mol, hereon referred to as conformations 1 and 2 (Figure 8B,C and Table
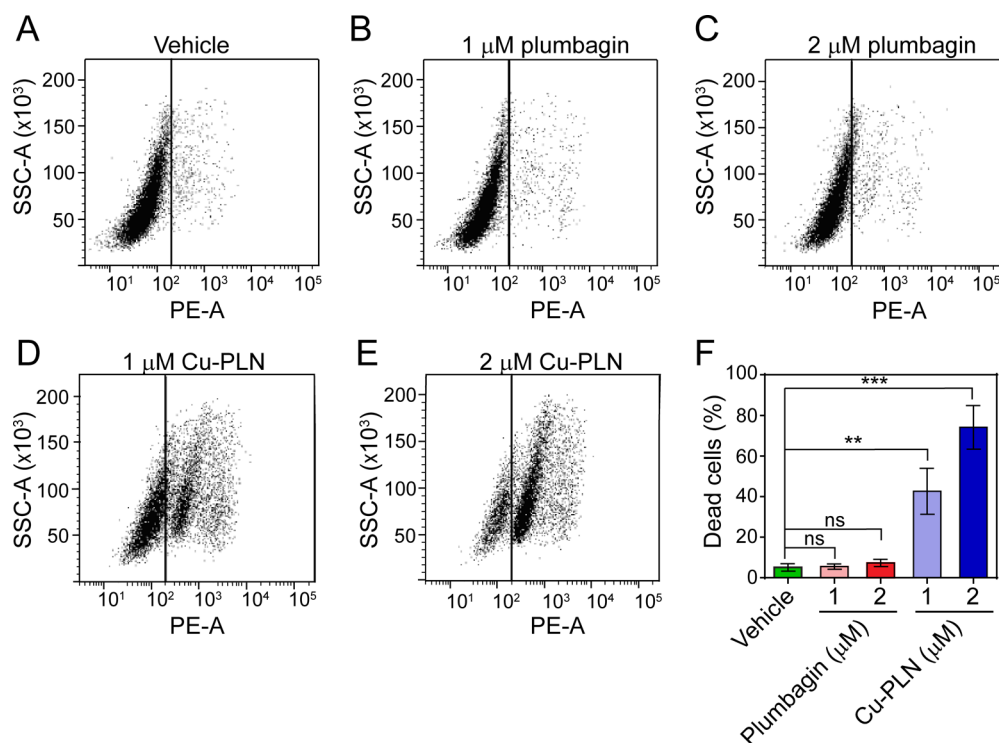
Figure 4. Cu-PLN treatment reduced the viability of HeLa cells. HeLa cells were incubated with vehicle [0.1% dimethyl sulfoxide (DMSO)], plumbagin, or Cu-PLN for 24 h. Cells were then stained with PI (50 μg/mL) and subjected to flow cytometry analysis. Representative dot plots of HeLa cells with (A) vehicle, (B) 1 μM plumbagin, (C) 2 μM plumbagin, (D) 1 μM Cu-PLN, and (E) 2 μM Cu-PLN are shown. (F) The percentage of dead cells was quantified from flow cytometry analysis. ns, $p > 0.05$; **, $p < 0.01$; ***, $p < 0.001$.

2). Both the conformations docked close to the colchicine-binding pocket, with conformation 1 docked at a distance of 10 Å from colchicine and conformation 2 at 5 Å. A close inspection of the binding pocket revealed the presence of similar residues near Cu-PLN and colchicine, indicating similar binding sites (Table 3). Conformation 1 made possible contacts with the residues of the T5-loop (Pro175) of α-tubulin and Asn329 of β-tubulin, whereas conformation 2 made contact with the residues of the T5-loop (Pro175) of α-tubulin and T7-loop (Gln247) and S9-strand (Thr353) of the β-tubulin chain (Figure 8B,C and Table 2). Residues of the T5-loop, T7-loop, and S9-strand are part of the colchicine-binding pocket.[26] In addition, T7-loop movement is reported to be important for the conformational change that occurs in the tubulin subunits during polymerization.[27] Cu-PLN, through its contact with the T7-loop, might hinder its movement, thus inhibiting tubulin polymerization. Also, as observed with conformation 2, the binding of Cu-PLN at the surface of the heterodimer interface might restrict the access of colchicine to its binding pocket, which is buried deep inside the interface (Figure 8D). In agreement with an earlier report,[18] plumbagin bound to tubulin at the colchicine-binding site with a binding energy of −7.0 kcal/mol (Figure 8E). The difference in the binding energies of Cu-PLN and plumbagin indicates that Cu-PLN has more affinity to tubulin than plumbagin.

Plumbagin is a colchicine-site binder,[18] and our docking analysis hinted that Cu-PLN might occupy the colchicine site on tubulin. To further strengthen this finding, we performed an in vitro competitive binding assay with Cu-PLN and colchicine. Colchicine fluoresces on binding to tubulin, and a decrease in colchicine-tubulin fluorescence was observed in the

presence of Cu-PLN (Figure 8F). Pre-incubation of tubulin with 5, 10, and 20 μM Cu-PLN inhibited the colchicine binding to tubulin by 24 ± 12, 51 ± 3, and 67 ± 3%, respectively (Figure 8G), indicating that Cu-PLN competes with colchicine for the same binding site. The inhibition of colchicine binding observed in this assay agrees with the docking results, which suggested that the binding of Cu-PLN near the colchicine site may restrict access to colchicine. Together, the data suggest that Cu-PLN is a colchicine-site binding agent.

Cu-PLN Induced DNA Damage in HeLa Cells. Microtubule-targeting agents and copper complexes are known to induce DNA damage in cancer cells.[9,28] Also, a previous study ascribed the cytotoxicity of Cu-PLN to its DNA binding and topoisomerase-1 inhibitory activity.[13] Therefore, we examined if Cu-PLN caused DNA damage in HeLa cells using an anti-γ-H2AX antibody. In comparison to the control, the fluorescence intensity of γ-H2AX did not increase upon treatment with 1 and 2 μM Cu-PLN for 2 h (Figure 9A). The increase in fluorescence of γ-H2AX was noticeable only after 4 h, which further substantially increased after 24 h of Cu-PLN treatment (Figure 9A). The intensity of γ-H2AX foci increased by 2.8 ($p < 0.05$) and 5-folds ($p < 0.001$) upon treatment with 1 μM Cu-PLN for 4 and 24 h with respect to the control cells (Figure 9B). Similarly, in the presence of 2 μM Cu-PLN, the intensity of γ-H2AX foci increased by 3 ($p < 0.05$) and 6.5-folds ($p < 0.001$) after 4 and 24 h of treatment (Figure 9B). The increase in γ-H2AX foci indicated that Cu-PLN causes double-stranded DNA damage in addition to microtubule depolymerization.

The effect of Cu-PLN on the cell cycle of HeLa cells was assessed by mitotic index calculation using phospho-histone H3 antibody, a mitotic cell marker.[29] The mitotic index was
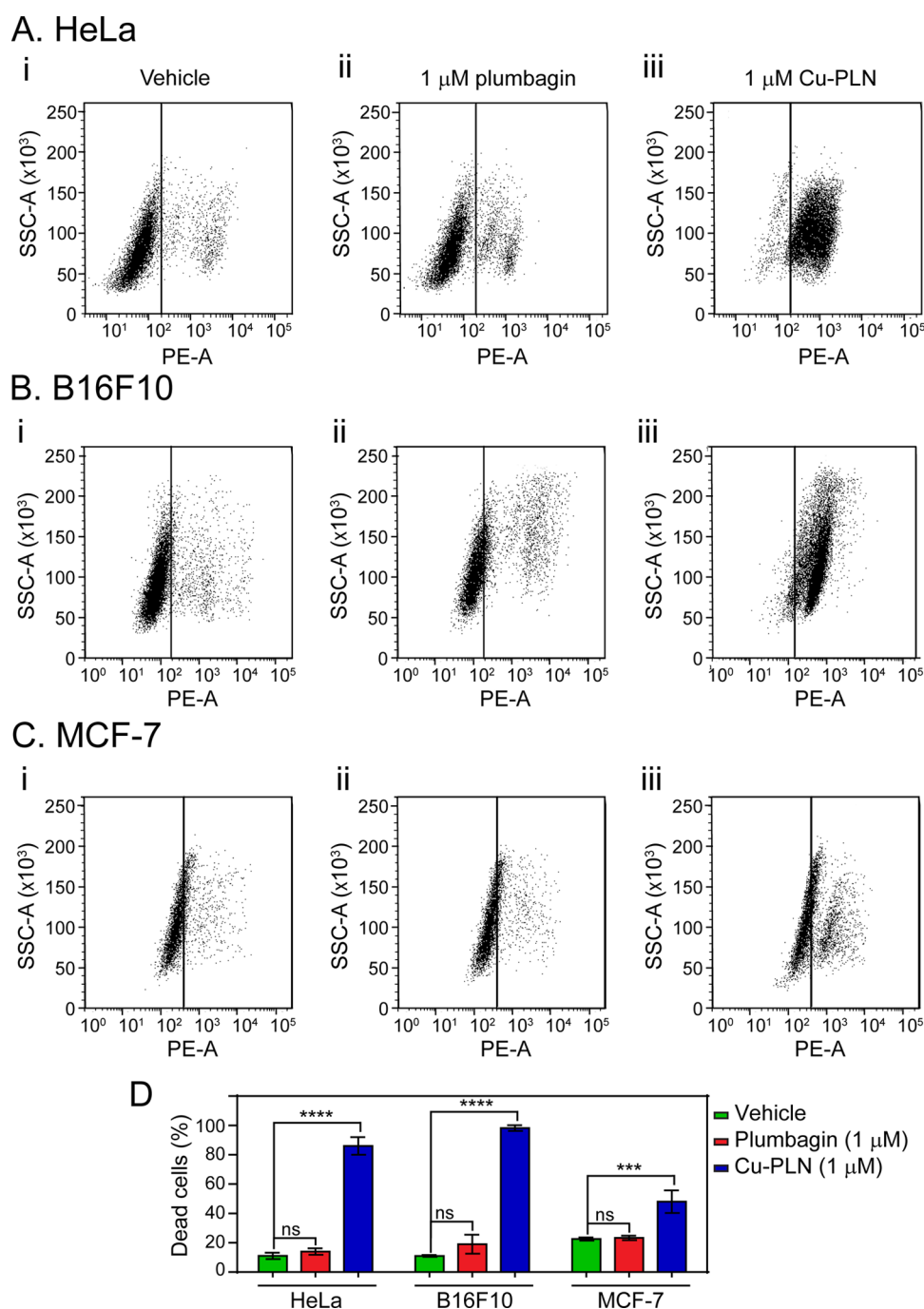
Figure 5. Cu-PLN exerted sustained cytotoxic effects in HeLa, B16F10, and MCF-7 cells. Cells were treated with vehicle (0.1% DMSO), 1 μM plumbagin, or 1 μM Cu-PLN for two cell cycles and then stained with PI (50 μg/mL). Representative dot plots of (A) HeLa, (B) B16F10, and (C) MCF-7 cells treated with (i) vehicle, (ii) 1 μM plumbagin, and (iii) 1 μM Cu-PLN are shown. (D) The percentage of dead cells was quantified from flow cytometry analysis. ns, $p > 0.05$; ***, $p < 0.001$; ****, $p < 0.0001$.

calculated as the ratio of the number of cells in mitosis to the total number of cells. The mitotic indexes of vehicle-treated, 0.85 and 1.7 μM Cu-PLN-treated cells were 5.1 $\pm$ 0.8, 5.2 $\pm$ 0.7, and 5.4 $\pm$ 0.5, respectively, suggesting that Cu-PLN did not induce a mitotic block in HeLa cells.

Cu-PLN Decreased the Mitochondrial Membrane Potential in HeLa Cells. A perturbation in the microtubule network has been shown to alter the mitochondrial membrane potential in cells.[30] Hence, we determined the effect of Cu-PLN on the mitochondrial membrane potential of HeLa cells using rhodamine 123 dye.[31] Cu-PLN significantly reduced the

fluorescence intensity of rhodamine 123 (Figure 10). In comparison to the control, the decrease in mitochondrial membrane potential was not significant ($p > 0.05$) after 2 h of incubation; however, after 4 h, the fluorescence intensity reduced from 0.092 $\pm$ 0.004 AU to 0.081 $\pm$ 0.003 AU ($p < 0.05$), and 0.076 $\pm$ 0.004 AU ($p < 0.01$) in the presence of 1 and 2 μM Cu-PLN, respectively (Figure 10). The fluorescence intensity strongly reduced after 24 h of Cu-PLN treatment, indicating that the metal complex effectively altered the mitochondrial membrane potential (Figure 10).
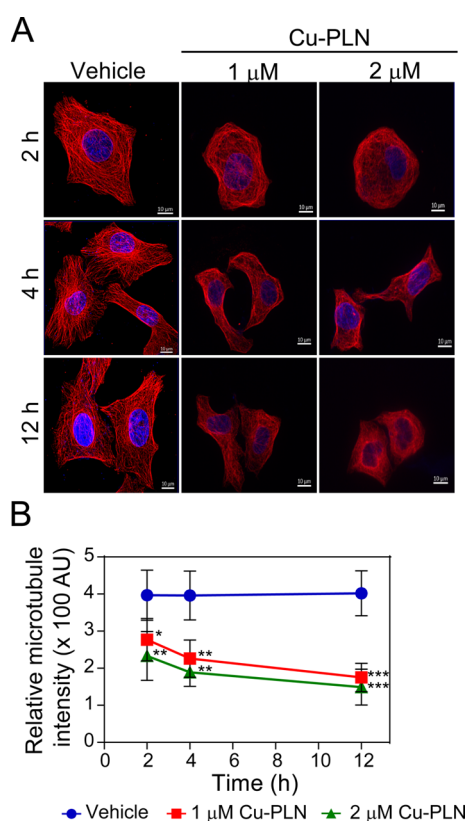
Figure 6. Cu-PLN treatment depolymerized microtubules in HeLa cells. (A) HeLa cells were incubated with vehicle (0.1% DMSO) or 1 and 2 μM Cu-PLN for 2, 4, and 12 h and then stained with α-tubulin antibody. The scale bar is 10 μm. (B) The fluorescence intensity of microtubules in the presence of vehicle (blue ●), 1 μM (red ■), and 2 μM (green ▲) Cu-PLN was quantified using 50 cells for each condition ($n = 3$). *, $p < 0.05$; **, $p < 0.01$; ***, $p < 0.001$.

Cu-PLN Induced ROS Production in HeLa Cells. Copper-based complexes trigger the production of ROS, causing a decrease in cell viability;[8] we therefore investigated if Cu-PLN triggered ROS production using DCFDA dye.[32,33] Cu-PLN treatment significantly increased the percentage of ROS-positive cells, as observed by an increase in DCFDA fluorescence (Figure 11). Incubation of HeLa cells with 1 and 2 μM Cu-PLN for 2, 4, and 24 h led to a time-dependent increase in the percentage of ROS-positive cells (Figure 11A–C). Notably, after 2 h of 1 and 2 μM Cu-PLN treatment, there were 31 ± 11% ($p < 0.01$) and 43 ± 9% ($p < 0.01$) ROS-positive cells, respectively, compared to the 1 ± 1% in vehicle-treated cells (Figure 11D and Table 4). The substantial increase in ROS-positive cells within 2 h of Cu-PLN treatment indicated that Cu-PLN might mediate its antiproliferative activity through ROS production.

Subsequently, we examined if ROS production is important for the anticancer activity of Cu-PLN using a thiol-based antioxidant N-acetyl cysteine (NAC), a precursor molecule for glutathione synthesis, that protects the cells from ROS-mediated damage.[34] The number of ROS-positive cells was higher when HeLa cells were treated with Cu-PLN alone (Figure 12A) than compared to cells pre-incubated with 1 mM NAC and then exposed to Cu-PLN (Figure 12B). There were 85 ± 11% ROS-positive cells when treated with 1 μM Cu-PLN and 40 ± 7% ($p < 0.01$) in cells pre-treated with NAC and then treated with 1 μM Cu-PLN (Figure 12C). Similarly, in
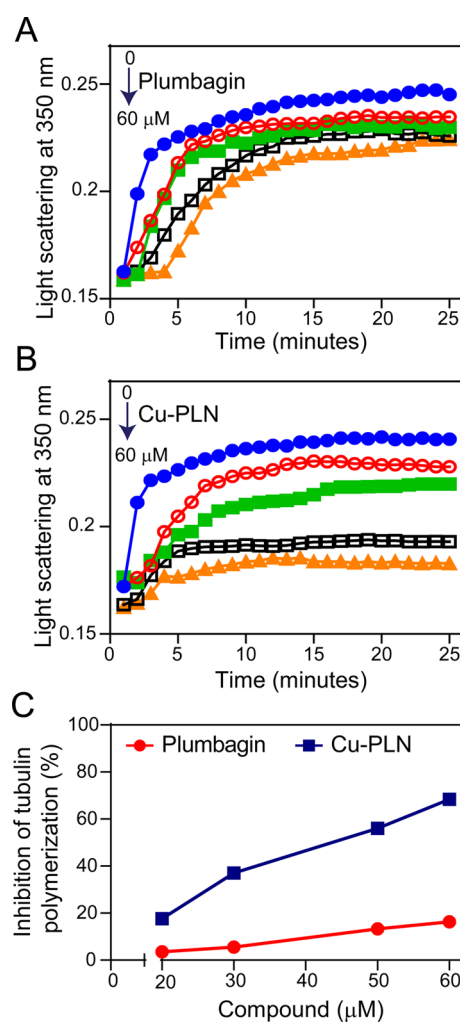

Figure 7. Cu-PLN inhibited taxol-induced tubulin polymerization. Tubulin (15 μM) was incubated in the absence (blue ●) or presence of 20 (red ○), 30 (green ■), 50 (□), and 60 (orange ▲) μM of (A) plumbagin or (B) Cu-PLN and then incubated with 5 μM taxol and 1 mM guanosine triphosphate (GTP). The polymerization of tubulin was monitored at 350 nm. (C) The percentage inhibition of tubulin polymerization in the presence of plumbagin (red ●) or Cu-PLN (blue ■) is shown.

the presence of 2 μM Cu-PLN, ROS-positive cells were 94 ± 4%, which reduced to 48 ± 9% ($p < 0.01$) in cells pre-treated with NAC (Figure 12C). These findings indicated that pre-treatment with NAC led to a decrease in Cu-PLN-mediated ROS production. We next checked the effect of NAC on the antiproliferative activity of Cu-PLN. In the absence of NAC, the IC$_{50}$ of Cu-PLN for HeLa cells was 0.9 ± 0.05 μM, while a pre-incubation with 1 mM NAC led to an increase in the IC$_{50}$ to 2.5 ± 0.1 μM (Figure 12D). The increase in the IC$_{50}$ of Cu-PLN in the presence of NAC indicates that the production of ROS plays an important role in the antiproliferative mechanism of Cu-PLN.

■ **DISCUSSION**

Several microtubule-targeting drugs, such as taxol, eribulin, vinblastine, vincristine, and estramustine, are successfully used to treat different cancers.[35,36] Plumbagin is known to depolymerize microtubules and inhibit cancer cell proliferation.[18] Our study shows that the copper complex of
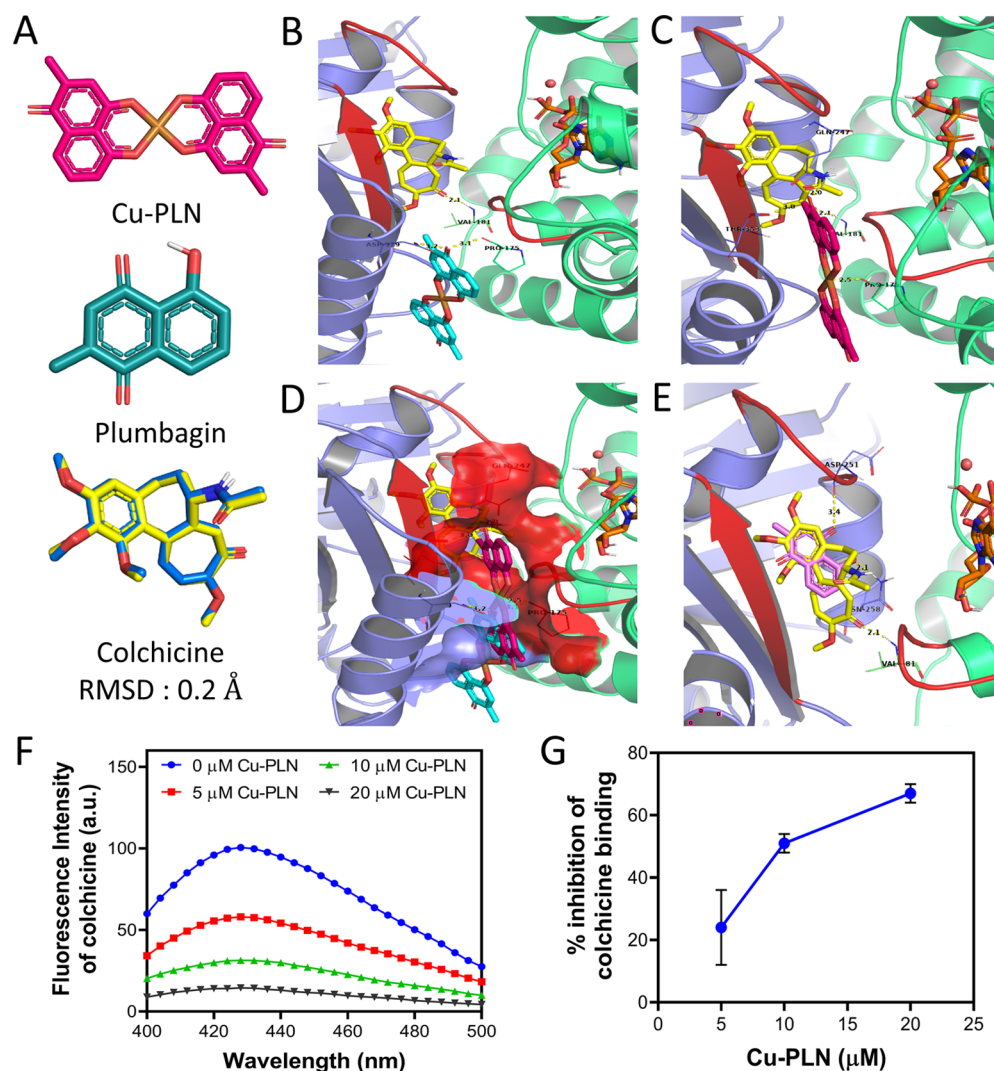
Figure 8. Cu-PLN bound to tubulin at the colchicine-binding site. (A) Structure of Cu-PLN and plumbagin. RMS deviation between the docked conformation and crystal structure of colchicine. The coordinates of the docked conformation of colchicine (yellow) were superimposed over the PDB coordinates of colchicine (blue) from the crystal structure 4O2B. (B-E) Cu-PLN and plumbagin docked at the interface of the tubulin heterodimer. Three-dimensional (3D) coordinates for the tubulin heterodimer were obtained from the crystal structure 4O2B. Color scheme: α-tubulin—lime green, β-tubulin—purple, GTP and guanosine 5′-diphosphate (GDP)—orange, and magnesium atom—salmon pink. Tubulin dimer is in cartoon representation, and all ligands are in stick representation. Red, blue, and white sticks represent oxygen, nitrogen, and hydrogen atoms, respectively. Possible hydrogen bonds are shown in yellow dotted lines. Cu-PLN docked at the interface of the $\alpha\beta$-tubulin heterodimer in two probable conformations; 1 (B, cyan) and 2 (C, magenta). The T5 loop, T7 loop, and S9 strand are in red. (D) Surface representation of residues within 4 Å of docked Cu-PLN conformations to show the binding pocket. (E) Plumbagin (pink) docked at the colchicine site overlapping with docked colchicine (yellow). (F) Fluorescence emission spectra of colchicine (10 μM) incubated with tubulin (5 μM) and 0 (blue ●), 5 (red ■), 10 green ▲), and 20 (gray ▼) μM Cu-PLN following excitation at 350 nm. (G) The percentage decrease in colchicine fluorescence at the emission maxima 430 nm in the presence of increasing concentrations of Cu-PLN.

plumbagin is a more effective anticancer agent than plumbagin with selective and sustained cytotoxicity mediated mainly through microtubule depolymerization and ROS production.

Possible Mechanism for the Antiproliferative Action of Cu-PLN. A short exposure of Cu-PLN disrupted the microtubule network in HeLa cells and the complex also strongly inhibited in vitro tubulin polymerization, indicating that Cu-PLN targets microtubules as its primary mode of exerting cytotoxicity toward cancer cells. The effect of Cu-PLN on microtubules can be based on the anti-tubulin activity of its ligand, plumbagin, that binds to tubulin, fragments microtubules into short protofilaments, and disrupts the cellular microtubule network.[18] The divalent copper in Cu-PLN forms square-planar coordination with two plumbagin molecules via

four O-atoms. The presence of planarity in tubulin-targeting compounds has been correlated with enhanced anticancer activity.[37] Therefore, the potent inhibition of tubulin polymerization and disassembly of microtubules in HeLa cells caused by Cu-PLN is possibly due to the presence of two plumbagin moieties in Cu-PLN, the geometry, and the hydrophobicity of the complex. Furthermore, a molecular docking analysis and biochemical assay indicated that Cu-PLN shares its binding site on tubulin with colchicine. Cu-PLN possibly binds strongly to tubulin at the colchicine site and causes disassembly of the microtubule network leading to a cascade of downstream effects, such as DNA damage, ROS generation, and mitochondrial membrane depolarization.

Table 2. Binding Energy and Interactions of Docked Cu-PLN, Colchicine, and Plumbagin with the Tubulin Heterodimer

docked compound	binding energy (kcal/mol)	interactions	
		residues involved	distance (Å)
Cu-PLN (conformation 1)	−9.8	Pro175A	3.1
		Asp329B	3.2
Cu-PLN (conformation 2)	−9.7	Pro175A	2.5
		Gln247B	2.0
		Thr353B	3.0
colchicine	−10.1	Val181A	2.1
plumbagin	−7.0	Asp251B	3.4
		Asn258B	2.1

Cu-PLN also triggered ROS production in HeLa cells. The generation of ROS can be ascribed to Cu-PLN-mediated microtubule disassembly and the presence of Cu^{2+} in the metal complex. Microtubule disassembly by microtubule-targeting agents, such as vinca alkaloids, nocodazole, and combretastatin-A4-phosphate, causes ROS accumulation.[38,39] In addition, a transient hyperpolarization of the mitochondrion can be caused by the tubulin-targeting activity of the microtubule-targeting agents, which releases pro-apoptotic factors from the mitochondria due to the collapse of the mitochondrial membrane potential $(\Delta\Psi_m)$, leading to apoptosis.[40] The presence of Cu^{2+} in Cu-PLN can also be responsible for ROS production. Reducing agents, such as glutathione, present at elevated concentrations in cancer cells[41] can reduce Cu^{2+} leading to the generation of intracellular superoxide radicals $(O_2^{\bullet-})$, causing cell death. Cu^{2+} complexes and glutathione have high oxidation and low reduction potentials, respectively.[42] The sharp difference in the oxidation potential of Cu^{2+}, present in Cu-PLN, and the reduction potential of glutathione may lead to rapid electron transport from glutathione onto the complex, converting Cu^{2+} into the radical ion, Cu^{+}.[42] These radical ions then react with water or oxygen, producing ROS. A similar electron transfer can occur between copper complexes and DNA, albeit to a lesser extent than glutathione.[42] As such, intercalation of Cu-PLN in the hydrophobic region of DNA may lead to ROS generation. In the present study, we observed that Cu-PLN induces DNA fragmentation in cultured cancer cells. Thus, the elevated concentration of ROS in the presence of Cu-PLN, combined with DNA intercalation and inhibition of topoisomerase I activity[13] might lead to Cu-PLN-mediated DNA damage.

Cu-PLN as a Potent Anticancer Agent. Cu-PLN showed potent anticancer activity against the proliferation of various cancer cells compared to plumbagin, which corroborates with the previous observations.[13,43] We also found out that the
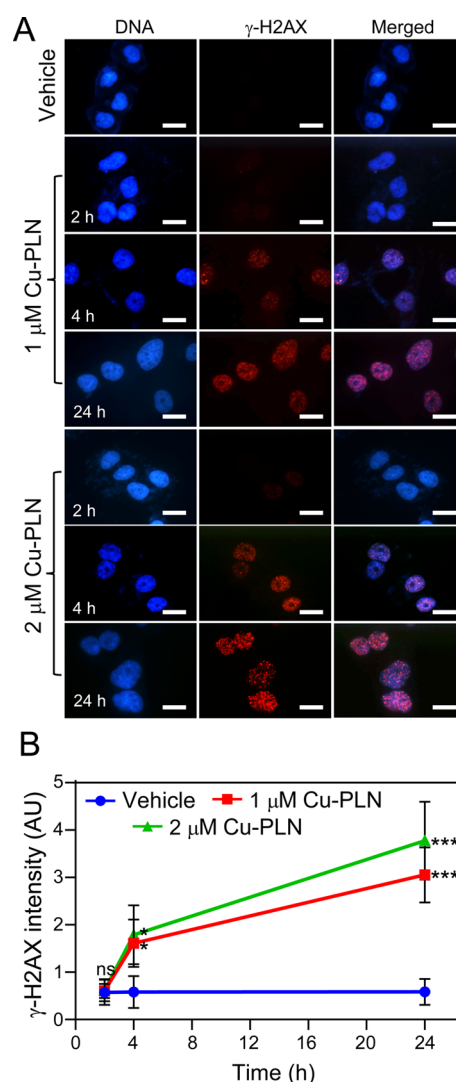

Figure 9. Treatment of HeLa cells with Cu-PLN led to DNA damage. (A) HeLa cells were incubated with vehicle (0.1% DMSO), 1 μM or 2 μM Cu-PLN for 2, 4, and 24 h. The cells were then immunostained with γ-H2AX antibody, and DNA was stained with Hoechst 33258. The scale bar is 10 μm. (B) γ-H2AX foci intensities for 100 cells were quantified in the presence of vehicle (blue ●), 1 (red ■), and 2 (green ▲) μM Cu-PLN. ns, $p > 0.05$; *, $p < 0.05$; ***, $p < 0.001$.

cytotoxic action of Cu-PLN is sustained and more selective toward cancer cells than plumbagin. The prolonged cytotoxicity of Cu-PLN might be due to the presence of copper and enhanced copper metabolism in cancer cells, which might have led to a higher accumulation of the metal complex in the target cells.[10,11] The selective activity of copper complexes against

Table 3. Residues Present in the Binding Pockets of Cu-PLN, Colchicine, and Plumbagin; Residues Common with the Colchicine-Binding Pocket Are in Bold

	residues of α-tubulin	residues of β-tubulin
Cu-PLN (conformation 1)	Pro175, Gln176	Asp329, Leu333, Gln336, Phe343, Val344, Glu345, Ile347, Pro348, Asn349, **Asn350, Val351, Lys352, Thr353**
Cu-PLN (conformation 2)	Pro175, Gln176, Val177, **Ser178, Thr179**, Tyr210, Arg214	Gln247, **Leu248**, Asp329, Leu333, Gln336, Asn349, **Val351, Lys352, Thr353, Ala354**
colchicine	Asn101, Ser178, Thr179, Ala180, Val181, Val182	Val238, Cys241, Leu242, Leu248, Ala250, Asp251, Leu252, Lys254, Leu255, Asn258, Met259, Thr314, Val315, Ala316, Ala317, Ile318, Asn350, Val351, Lys352, Thr353, Ala354, Ile378
plumbagin	**Asn101**	**Val238, Cys241, Leu248, Ala250, Asp251, Lys254, Leu255**, Ala256, **Asn258, Ala316, Ala317, Ile318, Lys352, Ala354**
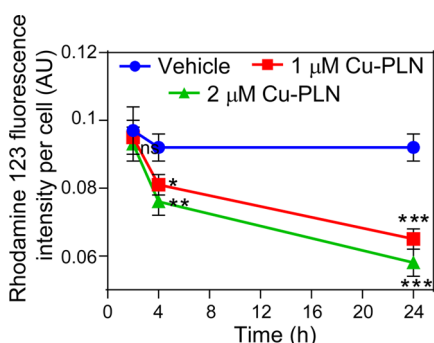
Figure 10. Cu-PLN decreased the mitochondrial membrane potential. HeLa cells were grown for 24 h and then incubated with vehicle (0.1% DMSO) (blue ●), 1 μM (red ■), or 2 μM (green ▲) Cu-PLN for another 2, 4, and 24 h. The cells were then stained with rhodamine 123, and the fluorescence was estimated by excitation at 488 nm and emission at 525 nm. ns, $p > 0.05$; *, $p < 0.05$; **, $p < 0.01$; ***, $p < 0.001$.

cancerous cells compared to noncancerous cells has been reported to be due to the enhanced copper metabolism and differences in p53 and androgen receptor expression levels in cancer cells.[10,44] The high accumulation of Cu-PLN could also be due to the permeability of the complex, as anticipated based on the log P (2.79) and TPSA (71.08 Å^2/molecule) values. The in silico determination of log P and TPSA predicts the permeability of a compound and is expected to be in the range of $-1 \leq$ to ≤ 3 (log P) and less than 140 Å^2 (TPSA) for good permeability.[24,25] The lipophilicity of Cu-PLN may enable higher retention of the compound inside cells leading to long-lasting cytotoxic effects. In addition, Cu-PLN was ~7 to 10 times more effective than cisplatin, a widely used anticancer agent. Cisplatin inhibits HeLa and MCF-7 cell proliferation with IC$_{50}$ of 8 $\pm$ 1 μM[45] and 16 $\pm$ 1 μM,[46] respectively, indicating that Cu-PLN displays more potent antiproliferative activity than cisplatin. The results suggest that Cu-PLN can be explored for antitumor applications.

■ MATERIALS AND METHODS

Growth Media and Chemicals. Plumbagin (5-hydroxy-2-methyl-1,4-naphthoquinone), 2′, 7′−dichlorofluorescein diacetate (DCFDA), PI, NAC, mouse monoclonal anti-α-tubulin IgG, GTP, taxol, colchicine, sulforhodamine B, Hoechst 33258, and rhodamine 123 dye were purchased from Sigma-Aldrich (USA). Copper chloride was procured from Merck (Germany). Anti-mouse Alexa 594 and fetal bovine serum (FBS) were purchased from Thermo Fisher Scientific (USA). Rabbit monoclonal anti-γ-H2AX IgG was purchased from Cell Signaling Technologies (USA). Dulbecco's Modified Eagle's medium (DMEM), antibiotic-antimycotic solution, and phosphate-buffered saline (PBS) were purchased from HiMedia (India). Sodium methoxide, methanol, and DMSO were obtained from Merck. All other reagents were procured either from Merck or HiMedia.

Interaction between Plumbagin and Cu²⁺. 25 μM solution of plumbagin was prepared in DMSO and titrated with increasing concentrations of CuCl$_2$ solution (2.5, 5, 12.5, 25, 35, 45, 50, 75, 100, 200, 300, 500, 750, and 1000 μM), also prepared in DMSO. Absorbance spectra were recorded in a JASCOV-730 spectrophotometer (JASCO, Japan) using a 1 cm path length cuvette in the range of 350−600 nm wavelength. The experiment was performed three times.

Synthesis of the Cu-PLN. Cu-PLN was synthesized through reflux and evaporation as described earlier.[13] Plumbagin (32 mg, 0.2 mmol) was dissolved in methanol containing 10 mg (0.2 mmol) sodium methoxide and incubated in shaking condition at 37 °C overnight. Subsequently, 16 mg (0.1 mmol) of CuCl$_2$ (dissolved in methanol) was added to the plumbagin solution dropwise and incubated overnight in shaking condition at 37 °C. Upon the addition of CuCl$_2$, the color changed from yellow to ruby red. The solution was then refluxed, followed by evaporation at 37 °C, resulting in dark red crystals of copper-plumbagin complex (Cu-PLN). For all experiments, Cu-PLN was dissolved in DMSO. The molar extinction coefficient (ε) of Cu-PLN was estimated by fitting the increase in absorbance at 530 nm due to the presence of Cu²⁺ to linear regression. The ε was determined to be 4800 M^{-1} cm^{-1} and was utilized to calculate the concentration of the metal complex.

Characterization of Cu-PLN. *High-Resolution Mass Spectrometry-Orbitrap.* The mass of Cu-PLN was estimated by the HRMS system (Thermo Scientific Q Exactive Orbitrap mass spectrometer fitted with Hypersil C18-column) in the positive ion mode. The mobile phase consisted of methanol and acetonitrile with 0.05% formic acid for 5 min at a flow rate of 150 μL/min. The sample injection volume was 5 μL.

Reverse Phase High-Pressure Liquid Chromatography. The purity of the synthesized compound was ascertained using an 1100 HPLC system (Agilent Technologies, USA), which consisted of an autosampler, C18 column, binary pump, and a diode array detector.[47] The column was washed thoroughly before each run using the mobile phase of 0.1% TFA in water (A) and 0.1% TFA in 50:50 (v/v) methanol/acetonitrile (B). Samples were analyzed at a fixed flow rate of 0.2 mL/min in the gradient analysis mode. The chromatograms were analyzed in Agilent ChemStation.

FTIR Spectroscopy. FTIR spectra of CuCl$_2$, plumbagin, and Cu-PLN were recorded in KBr pellets at 4 cm^{-1} resolution in an infrared spectrometer (JASCO FTIR 4700). For each sample, 32 scans were performed in the range of 4000 to 450 cm^{-1}. After the acquisition, raw spectra were subjected to CO$_2$ correction and smoothing in the instrument software.

X-ray Diffraction Analysis. The crystal structure of a single crystal of Cu-PLN was obtained from a Rigaku Saturn 724+ charge-coupled device Single Crystal X-ray diffractometer equipped with monochromator Cu and Mo Kα (wavelength = 0.71075 Å). Initially, a crystal of Cu-PLN was obtained from the mother liquor, soaked in silicone oil, and subsequently mounted on a glass fiber tip. The data integration was made using CrysAlis. The crystal structure was resolved and refined as described previously using Olex, ShelXL-2016/6, and EnCIFer.[48−51]

Cell Culture. Human cervical carcinoma (HeLa), human breast cancer (MCF-7), normal human mammary epithelial cells (MCF10A), murine melanoma (B16F10), and murine fibroblast (L929) cell lines were procured from the National Centre for Cell Sciences, Pune, India. The cells were grown in DMEM supplemented with 10% (v/v) FBS and 1% (v/v) antibiotic-antimycotic solution. MCF10A was grown as mentioned earlier.[28] All the cells were maintained at 37 °C in a humidified incubator (Sanyo, Japan) supplemented with 5% CO$_2$.

Determination of Half-Maximal Inhibitory Concentration (IC$_{50}$). HeLa, MCF-7, MCF10A, B16F10, and L929 cells were grown at a density of 1 × 10^4 cells/well in 96-well cell culture
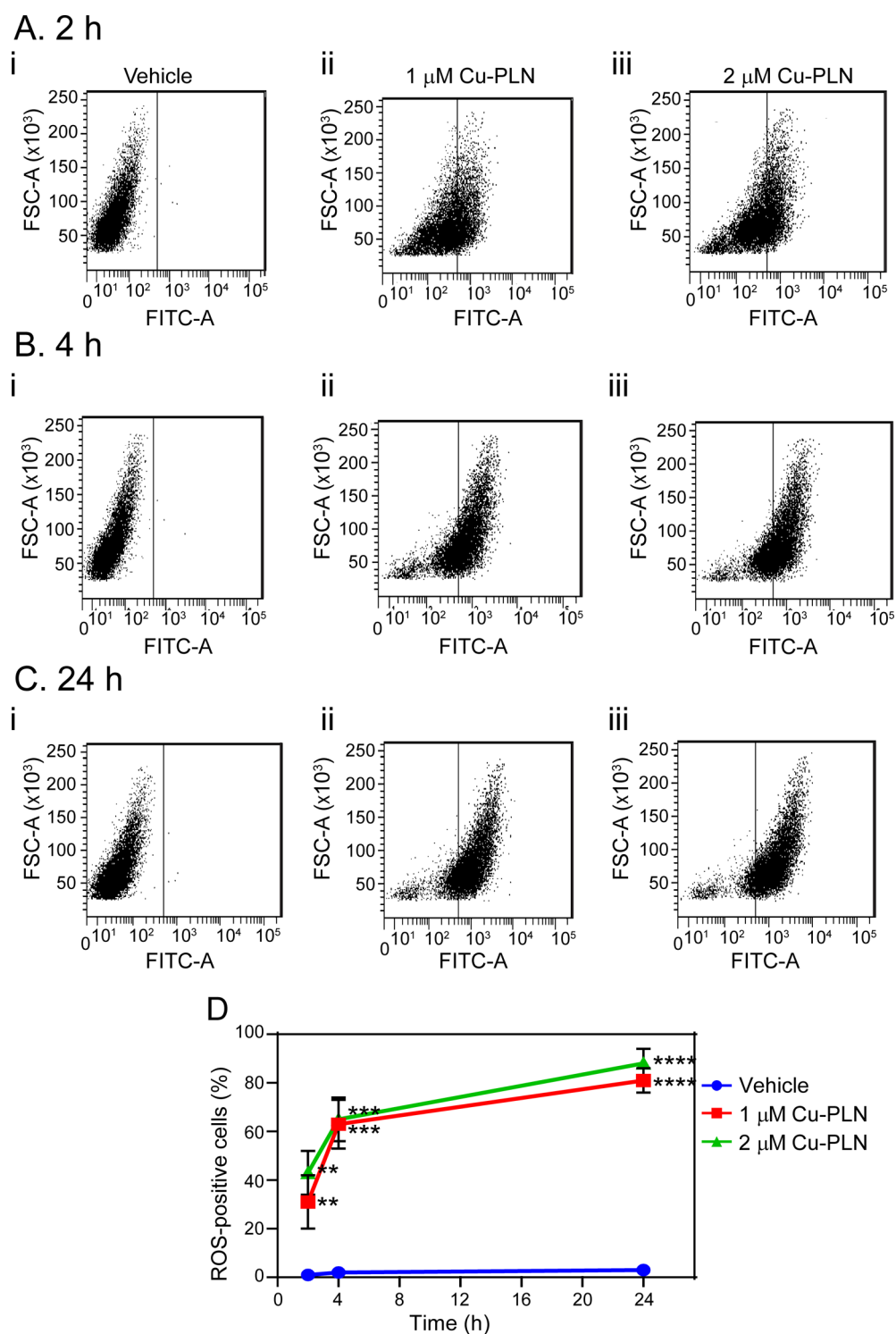
Figure 11. Cu-PLN induced ROS production in HeLa cells. HeLa cells were treated with vehicle (0.1% DMSO), 1, or 2 μM Cu-PLN for 2, 4, and 24 h. The cells were then stained with 5 μM DCFDA and subjected to flow cytometry. Representative dot plots of HeLa cells incubated for (A) 2 h, (B) 4 h, and (C) 24 h with (i) vehicle, (ii) 1 μM Cu-PLN, and (iii) 2 μM Cu-PLN are shown. (D) Percentage of ROS-positive cells plotted over time for vehicle (blue ●), 1 (red ■), and 2 (green ▲) μM Cu-PLN. **, $p < 0.01$; ***, $p < 0.001$; ****, $p < 0.0001$.

plates and then incubated with different concentrations of either plumbagin or Cu-PLN for one cell cycle. The cells were processed for Sulforhodamine B assay as described earlier,[52] and IC_{50} values were calculated using GraphPad Prism software version 6.0 (GraphPad Software, USA) by fitting the values in a nonlinear regression equation as described

earlier.[52] Three independent experiments were performed for each of the cell lines.

Similarly, the effect of NAC on the antiproliferative activity of Cu-PLN was determined in HeLa cells. Cells were initially treated with 1 mM NAC for 1 h at 37 °C, followed by incubation with different concentrations of Cu-PLN for one cell cycle. The cells were processed for Sulforhodamine B

**Table 4. Cu-PLN Treatment Increased ROS Generation in HeLa Cells**

	% ROS-positive cells		
	2 h	4 h	24 h
control	1 ± 1	2 ± 1	3 ± 1
1 μM Cu-PLN	31 ± 11	63 ± 10	81 ± 5
2 μM Cu-PLN	43 ± 9	65 ± 9	88 ± 6

assay, and IC$_{50}$ was determined. The experiment was performed three times.

Determination of Cell Viability. HeLa cells were incubated for one or two cell cycles, and MCF-7 and B16F10 cells were incubated for two cell cycles with vehicle (0.1% DMSO), plumbagin, or Cu-PLN. The cells were trypsinized and washed with PBS twice. Cells were then incubated in the dark with PI (50 μg/mL) at room temperature for 30 min. The data were acquired using a BD FACSAria flow cytometer (Becton

Dickinson, USA) and analyzed in FlowJo software. 10 000 cells were considered in each case, and the experiment was performed three times.

Immunofluorescence Analysis. Immunofluorescence analysis of microtubules in the absence and presence of Cu-PLN was performed as described earlier.[53,54] Briefly, HeLa cells (25 000 cells/well) were seeded on coverslips and incubated in the presence of vehicle (0.1% DMSO), 1 or 2 μM Cu-PLN for 2, 4, and 12 h. The cells were then fixed using 3.7% formaldehyde and permeabilized using 100% chilled methanol. Then, the control and Cu-PLN treated cells were incubated with α-tubulin antibody (1:400) to visualize microtubules, followed by a suitable secondary antibody. Nuclear DNA was stained with 10 μg/mL Hoechst 33258. The cells were then imaged in a confocal spinning-disk microscope CSU-X1(Yokogawa, Japan), and the fluorescence intensities of microtubules in control and treated groups were quantified using Zen software.
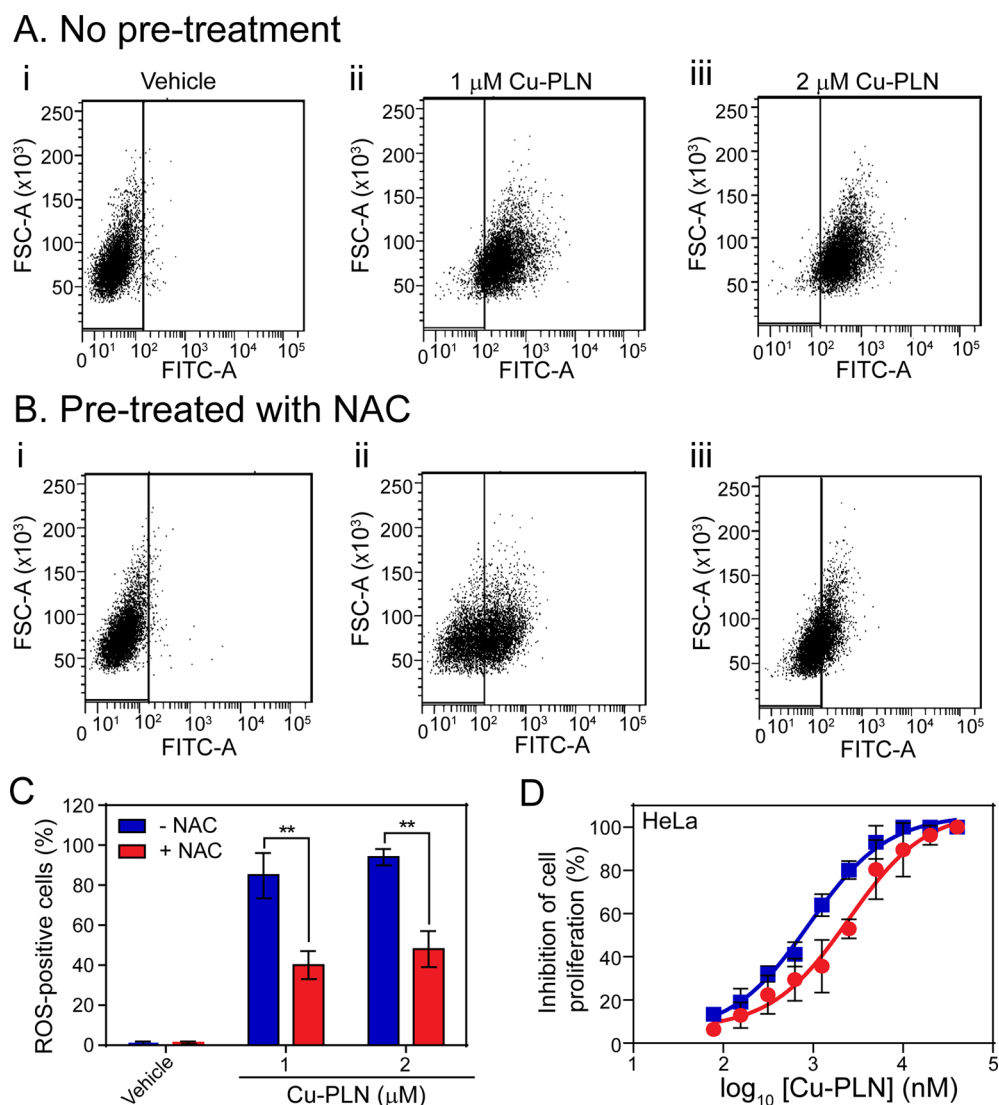
Figure 12. Pre-treatment with NAC reduces ROS production and antiproliferative activity of Cu-PLN. HeLa cells were pre-treated with 1 mM NAC for 1 h and then treated with vehicle (0.1% DMSO), 1 μM, or 2 μM Cu-PLN for 24 h. The cells were then stained with 5 μM DCFDA and subjected to flow cytometry. Representative dot plots of HeLa cells pre-treated without (A) or with (B) 1 mM NAC and then treated with (i) vehicle, (ii) 1 μM Cu-PLN, and (iii) 2 μM Cu-PLN are shown. (C) Percentage of ROS-positive cells induced by Cu-PLN without or with 1 mM NAC pre-treatment. ** denotes $p < 0.01$. (D) IC$_{50}$ of Cu-PLN in HeLa cells pre-treated without (blue ■) or with (red ●) 1 mM NAC.

In each set, 50 cells were quantified for each case, and three independent experiments were performed.

Effect of Cu-PLN on Taxol-Induced Tubulin Polymerization. Tubulin was isolated from the goat brain tissue as reported earlier.[55,56] Purified tubulin (15 μM) was incubated without or with different concentrations (20, 30, 50, and 60 μM) of either plumbagin or Cu-PLN in PEM buffer (25 mM PIPES, 1 mM EGTA, and 3 mM MgCl$_2$, pH 6.8) on ice for 10 min. Subsequently, 5 μM taxol and 1 mM GTP were added to the reaction mixture. The kinetics of tubulin assembly was monitored by light scattering at 350 nm at 37 °C for 25 min using Spectramax M2^e (Molecular Devices, USA). The experiment was performed three times.

Molecular Docking Analysis. The docking of Cu-PLN, plumbagin, and colchicine on the tubulin heterodimer was performed using AutoDock Vina.[57] 3D coordinates of tubulin and colchicine were obtained from the PDB ID 4O2B.[26] For the tubulin heterodimer, chains A and B, along with GDP, GTP, and magnesium atoms, were kept, and other chains were deleted. 3D coordinates of Cu-PLN were obtained from the crystal structure, and plumbagin's 3D coordinates were obtained from the PRODRG server.[58] The macromolecule and ligand structures were prepared using the MGL Tools as per the manual.[59] Initially, blind docking was performed by covering the entire protein structure in a grid box of 66 × 106 × 94 with a spacing of 1 Å. The lowest energy conformations bound at the interface of the heterodimer. Therefore, local docking was performed at the interface with a grid box of 26 × 28 × 34, spacing 1 Å. Five independent dockings were performed by changing the initial coordinates of the ligand. The lowest energy conformation was considered as the final binding mode. The docked protein–ligand complex was further analyzed in PyMOL 2.4.1.[60] Using the same parameters, colchicine and plumbagin were also docked, and the root mean square deviation for colchicine was determined using UCSF Chimera version 1.11.[61]

Competition Assay with Colchicine. Tubulin (5 μM) was incubated without or with Cu-PLN (5, 10, and 20 μM) in 25 mM PIPES (pH 6.8) for 15 min on ice. Subsequently, colchicine (10 μM) was added, and the reaction mixture was further incubated at 37 °C for 45 min. The fluorescence emission spectra of colchicine were recorded by exciting the mixture at 350 nm in a spectrofluorometer (JASCO 8500). The emission spectra of samples with Cu-PLN and colchicine without tubulin were blank. The inner filter effect correction was performed as described earlier,[62] and the percentage inhibition of colchicine binding to tubulin was plotted. The experiment was performed three times.

Effect of Cu-PLN on DNA. HeLa cells were incubated with vehicle (0.1% DMSO), 1 or 2 μM Cu-PLN for 2, 4, and 24 h. Subsequently, the cells were washed twice with PBS, immunostained with γ-H2AX antibody (1:400) and then stained with Hoechst 33258. Then, the vehicle- and Cu-PLN-treated HeLa cells were visualized in an epifluorescent microscope Eclipse TE 2000U (Nikon, Japan). The fluorescence intensity of 100 cells was quantified in each case using ImageJ software, and the experiment was performed three times.

Mitotic Index Calculation. The effect of Cu-PLN on the cell cycle of HeLa cells was determined using phospho-histone H3 staining as described earlier.[31] HeLa cells were treated with 0.85 and 1.7 μM of Cu-PLN for 18 h and then immunostained with anti-phospho-histone H3 and FITC-conjugated secon-

dary antibodies. DNA was stained with Hoechst. The cells were visualized under an Eclipse TE 2000U microscope (Nikon, Japan) at 40× magnification. The experiment was performed three times, and 500 cells were counted in each case.

Determination of Mitochondrial Membrane Potential in the Presence of Cu-PLN. HeLa cells (25 000 cells/well) were seeded in a 24-well plate and incubated for 24 h. The cells were treated either with the vehicle (0.1% DMSO) or 1 and 2 μM Cu-PLN for 2, 4, and 24 h. Later, the cells were stained using 1 μM rhodamine 123 dye for 30 min in the dark. The fluorescence intensities were then recorded with an excitation wavelength of 488 nm and an emission wavelength of 525 nm using SpectraMax M2^e. Simultaneously, the number of cells per well was determined using trypan blue dye for each experimental condition. The fluorescence intensities obtained were then normalized, considering the number of cells in each well. The experiment was performed three times.

Detection of ROS in the Presence of Cu-PLN. HeLa cells were incubated either with the vehicle (0.1% DMSO) or with 1 or 2 μM Cu-PLN for different durations. The cells were then trypsinized, washed twice with PBS, and further incubated with 5 μM DCFDA for 30 min in the dark. The cells were centrifuged at 3000 rpm for 10 min, washed twice with PBS, and the cell pellet was then resuspended in PBS and subjected to flow cytometry analysis. The fluorescence intensities of 10 000 cells were accounted for the determination of the average fluorescence intensity in each experimental case. The experiment was performed three times.

Similarly, the effect of pre-treatment with NAC on ROS production in the presence of Cu-PLN was determined. HeLa cells were incubated in the absence or presence of 1 mM NAC for 1 h. Subsequently, the cells were washed with PBS and incubated with vehicle (0.1% DMSO), 1, or 2 μM Cu-PLN for 24 h. The cells were then trypsinized, washed twice with PBS, and incubated with 5 μM DCFDA for 30 min in the dark. The cells were then centrifuged and subjected to flow cytometry analysis. The fluorescence intensities of 10 000 cells were considered in each experimental case. The experiment was performed three times.

Statistical Analysis. Data are represented as mean ± standard deviation. Student's *t*-test (GraphPad software) was used to determine the significance of the data, and a $p \leq 0.05$ was considered significant.

■ ASSOCIATED CONTENT

Data Availability Statement

All data described here are available from the corresponding author on reasonable request.

ⓈⒾ Supporting Information

The Supporting Information is available free of charge at https://pubs.acs.org/doi/10.1021/acsomega.2c06691.

> Crystal structure of Cu-PLN and crystal data and structure refinement for Cu-PLN (PDF)

■ AUTHOR INFORMATION

Corresponding Author

Dulal Panda − *Department of Biosciences and Bioengineering, Indian Institute of Technology Bombay, Mumbai 400076, India; National Institute of Pharmaceutical Education and Research, SAS Nagar, Punjab 160062, India;* ⊙ orcid.org/

0000-0002-9885-4500; Email: panda@iitb.ac.in, panda@niper.ac.in

Authors

Sandipan Mukherjee − *Department of Biosciences and Bioengineering, Indian Institute of Technology Bombay, Mumbai 400076, India;* ⦿ orcid.org/0000-0002-3274-7622

Avishkar V. Sawant − *Department of Biosciences and Bioengineering, Indian Institute of Technology Bombay, Mumbai 400076, India*

Shweta S. Prassanawar − *Department of Biosciences and Bioengineering, Indian Institute of Technology Bombay, Mumbai 400076, India*

Complete contact information is available at:
https://pubs.acs.org/10.1021/acsomega.2c06691

Author Contributions

§S.M. and A.V.S. contributed equally.

Notes

The authors declare no competing financial interest.

■ REFERENCES

(1) Barry, N. P. E.; Sadler, P. J. Exploration of the medical periodic table: towards new targets. *Chem. Commun.* **2013**, *49*, 5106−5131.

(2) Renfrew, A. K. Transition metal complexes with bioactive ligands: mechanisms for selective ligand release and applications for drug delivery. *Metallomics* **2014**, *6*, 1324−1335.

(3) Boros, E.; Dyson, P. J.; Gasser, G. Classification of metal-based drugs according to their mechanisms of action. *Chem* **2020**, *6*, 41−60.

(4) Dilruba, S.; Kalayda, G. v. Platinum-based drugs: past, present and future. *Cancer Chemother. Pharmacol.* **2016**, *77*, 1103−1124.

(5) Rabik, C. A.; Dolan, M. E. Molecular mechanisms of resistance and toxicity associated with platinating agents. *Cancer Treat Rev.* **2007**, *33*, 9−23.

(6) Lazarević, T.; Rilak, A.; Bugarčić, Ž. D. Platinum, palladium, gold and ruthenium complexes as anticancer agents: Current clinical uses, cytotoxicity studies and future perspectives. *Eur. J. Med. Chem.* **2017**, *142*, 8−31.

(7) Yousuf, I.; Bashir, M.; Arjmand, F.; Tabassum, S. Advancement of metal compounds as therapeutic and diagnostic metallodrugs: Current frontiers and future perspectives. *Coord. Chem. Rev.* **2021**, *445*, 214104.

(8) Zehra, S.; Tabassum, S.; Arjmand, F. Biochemical pathways of copper complexes: Progress over the past 5 years. *Drug Discov. Today* **2021**, *26*, 1086−1096.

(9) Santini, C.; Pellei, M.; Gandin, V.; Porchia, M.; Tisato, F.; Marzano, C. Advances in copper complexes as anticancer agents. *Chem. Rev.* **2014**, *114*, 815−862.

(10) Oliveri, V. Selective targeting of cancer cells by copper ionophores: An Overview. *Front. Mol. Biosci.* **2022**, *9*, 841814.

(11) da Silva, D. A.; De Luca, A.; Squitti, R.; Rongioletti, M.; Rossi, L.; Machado, C. M. L.; Cerchiaro, G. Copper in tumors and the use of copper-based compounds in cancer treatment. *J. Inorg. Biochem.* **2022**, *226*, 111634.

(12) Barilli, A.; Atzeri, C.; Bassanetti, I.; Ingoglia, F.; Dall'Asta, V.; Bussolati, O.; Maffini, M.; Mucchino, C.; Marchiò, L. Oxidative stress induced by copper and iron complexes with 8-hydroxyquinoline derivatives causes paraptotic death of HeLa cancer cells. *Mol. Pharm.* **2014**, *11*, 1151−1163.

(13) Chen, Z.-F.; Tan, M.-X.; Liu, L.-M.; Liu, Y.-C.; Wang, H.-S.; Yang, B.; Peng, Y.; Liu, H.-G.; Liang, H.; Orvig, C. Cytotoxicity of the traditional Chinese medicine (TCM) plumbagin in its copper chemistry. *Dalton Trans.* **2009**, *48*, 10824−10833.

(14) Checker, R.; Sharma, D.; Sandur, S. K.; Khanam, S.; Poduval, T. B. Anti-inflammatory effects of plumbagin are mediated by inhibition of NF-KappaB activation in lymphocytes. *Int. Immunopharmacol.* **2009**, *9*, 949−958.

(15) Padhye, S.; Dandawate, P.; Yusufi, M.; Ahmad, A.; Sarkar, F. H. Perspectives on medicinal properties of plumbagin and its analogs. *Med. Res. Rev.* **2012**, *32*, 1131−1158.

(16) Bhattacharya, A.; Jindal, B.; Singh, P.; Datta, A.; Panda, D. Plumbagin inhibits cytokinesis in Bacillus subtilis by inhibiting FtsZ assembly - a mechanistic study of its antibacterial activity. *FEBS J.* **2013**, *280*, 4585−4599.

(17) Tripathi, S. K.; Panda, M.; Biswal, B. K. Emerging role of plumbagin: cytotoxic potential and pharmaceutical relevance towards cancer therapy. *Food Chem. Toxicol.* **2019**, *125*, 566−582.

(18) Acharya, B. R.; Bhattacharyya, B.; Chakrabarti, G. The natural naphthoquinone plumbagin exhibits antiproliferative activity and disrupts the microtubule network through tubulin binding. *Biochemistry* **2008**, *47*, 7838−7845.

(19) Inbaraj, J. J.; Chignell, C. F. Cytotoxic action of juglone and plumbagin: a mechanistic study using HaCaT keratinocytes. *Chem. Res. Toxicol.* **2004**, *17*, 55−62.

(20) Ramirez, O.; Motta-Mena, L. B.; Cordova, A.; Garza, K. M. A small library of synthetic di-substituted 1, 4-naphthoquinones induces ROS-mediated cell death in murine fibroblasts. *PLoS One* **2014**, *9*, No. e106828.

(21) Sagar, S.; Esau, L.; Moosa, B.; Khashab, N. M.; Bajic, V. B.; Kaur, M. Cytotoxicity and apoptosis induced by a plumbagin derivative in estrogen positive MCF-7 breast cancer cells. *Anticancer Agents Med. Chem.* **2014**, *14*, 170−180.

(22) Sumsakul, W.; Plengsuriyakarn, T.; Na-Bangchang, K. Pharmacokinetics, toxicity, and cytochrome P450 modulatory activity of plumbagin. *BMC Pharmacol. Toxicol.* **2016**, *17*, 1−10.

(23) Pawar, A.; Patel, R.; Arulmozhi, S.; Bothiraja, C. d-α-Tocopheryl polyethylene glycol 1000 succinate conjugated folic acid nanomicelles: towards enhanced bioavailability, stability, safety, prolonged drug release and synergized anticancer effect of plumbagin. *RSC Adv.* **2016**, *6*, 78106−78121.

(24) Veber, D. F.; Johnson, S. R.; Cheng, H.-Y.; Smith, B. R.; Ward, K. W.; Kopple, K. D. Molecular properties that influence the oral bioavailability of drug candidates. *J. Med. Chem.* **2002**, *45*, 2615−2623.

(25) Klein-Júnior, L. C.; Corrêa, R.; Vander Heyden, Y.; Cechinel Filho, V. All that glitters is not gold: panning cytotoxic natural products and derivatives with a fused tricyclic backbone by the estimation of their leadlikeness for cancer treatment. *Eur. J. Med. Chem.* **2019**, *166*, 1−10.

(26) Prota, A. E.; Danel, F.; Bachmann, F.; Bargsten, K.; Buey, R. M.; Pohlmann, J.; Reinelt, S.; Lane, H.; Steinmetz, M. O. The novel microtubule-destabilizing drug BAL27862 binds to the colchicine site of tubulin with distinct effects on microtubule organization. *J. Mol. Biol.* **2014**, *426*, 1848−1860.

(27) Dorléans, A.; Gigant, B.; Ravelli, R. B. G.; Mailliet, P.; Mikol, V.; Knossow, M. Variations in the colchicine-binding domain provide

insight into the structural switch of tubulin. *Proc. Natl. Acad. Sci. U.S.A.* **2009**, *106*, 13775−13779.

(28) Poruchynsky, M. S.; Komlodi-Pasztor, E.; Trostel, S.; Wilkerson, J.; Regairaz, M.; Pommier, Y.; Zhang, X.; Kumar Maity, T.; Robey, R.; Burotto, M.; Sackett, D.; Guha, U.; Fojo, A. T. Microtubule-targeting agents augment the toxicity of DNA-damaging agents by disrupting intracellular trafficking of DNA repair proteins. *Proc. Natl. Acad. Sci. U.S.A.* **2015**, *112*, 1571−1576.

(29) Wei, Y.; Mizzen, C. A.; Cook, R. G.; Gorovsky, M. A.; Allis, C. D. Phosphorylation of histone H3 at Serine 10 is correlated with chromosome condensation during mitosis and meiosis in Tetrahymena. *Proc. Natl. Acad. Sci. U.S.A.* **1998**, *95*, 7480−7484.

(30) Maldonado, E. N.; Patnaik, J.; Mullins, M. R.; Lemasters, J. J. Free tubulin modulates mitochondrial membrane potential in cancer cells. *Cancer Res.* **2010**, *70*, 10192−10201.

(31) Kumari, A.; Srivastava, S.; Manne, R. K.; Sisodiya, S.; Santra, M. K.; Guchhait, S. K.; Panda, D. C12, a combretastatin-A4 analog, exerts anticancer activity by targeting microtubules. *Biochem. Pharmacol.* **2019**, *170*, 113663.

(32) Wu, D.; Yotnda, P. Production and detection of reactive oxygen species (ROS) in cancers. *J. Visualized Exp.* **2011**, *57*, No. e3357.

(33) Hura, N.; Sawant, A. v.; Kumari, A.; Guchhait, S. K.; Panda, D. Combretastatin-inspired heterocycles as antitubulin anticancer agents. *ACS Omega* **2018**, *3*, 9754−9769.

(34) Viola-Rhenals, M.; Rieber, M. S.; Rieber, M. Suppression of survival in human SKBR3 breast carcinoma in response to metal-chelator complexes is preferential for copper-dithiocarbamate. *Biochem. Pharmacol.* **2006**, *71*, 722−734.

(35) Steinmetz, M. O.; Prota, A. E. Microtubule-targeting agents: strategies to hijack the cytoskeleton. *Trends Cell Biol.* **2018**, *28*, 776−792.

(36) Čermák, V.; Dostál, V.; Jelínek, M.; Libusová, L.; Kovář, J.; Rösel, D.; Brábek, J. Microtubule-targeting agents and their impact on cancer treatment. *Eur. J. Cell Biol.* **2020**, *99*, 151075.

(37) Wittmann, C.; Sivchenko, A. S.; Bacher, F.; Tong, K. K. H.; Guru, N.; Wilson, T.; Gonzales, J.; Rauch, H.; Kossatz, S.; Reiner, T.; Babak, M. V.; Arion, V. B. Inhibition of microtubule dynamics in cancer cells by indole-modified latonduine derivatives and their metal complexes. *Inorg. Chem.* **2022**, *61*, 1456−1470.

(38) Petit, I.; Karajannis, M. A.; Vincent, L.; Young, L.; Butler, J.; Hooper, A. T.; Shido, K.; Steller, H.; Chaplin, D. J.; Feldman, E.; Rafii, S. The microtubule-targeting agent CA4P regresses leukemic xenografts by disrupting interaction with vascular cells and mitochondrial-dependent cell death. *Blood* **2008**, *111*, 1951−1961.

(39) Chiu, W.-H.; Luo, S.-J.; Chen, C.-L.; Cheng, J.-H.; Hsieh, C.-Y.; Wang, C.-Y.; Huang, W.-C.; Su, W.-C.; Lin, C.-F. Vinca alkaloids cause aberrant ROS-mediated JNK activation, Mcl-1 downregulation, DNA damage, mitochondrial dysfunction, and apoptosis in lung adenocarcinoma cells. *Biochem. Pharmacol.* **2012**, *83*, 1159−1171.

(40) Pasquier, E.; Carré, M.; Pourroy, B.; Camoin, L.; Rebaï, O.; Briand, C.; Braguer, D. Antiangiogenic activity of paclitaxel is associated with its cytostatic effect, mediated by the initiation but not completion of a mitochondrial apoptotic signaling pathway. *Mol. Cancer Ther.* **2004**, *3*, 1301−1310.

(41) Bansal, A.; Simon, M. C. Glutathione metabolism in cancer progression and treatment resistance. *J. Cell Biol.* **2018**, *217*, 2291−2298.

(42) Miao, T.; Deng, Q.; Gao, H.; Fu, X.; Li, S. Theoretical Studies on DNA-Cleavage Mechanism of Copper(II) Complexes: Probing Generation of Reactive Oxygen Species. *J. Chem. Inf. Model.* **2018**, *58*, 859−866.

(43) Wehbe, M.; Lo, C.; Leung, A. W. Y.; Dragowska, W. H.; Ryan, G. M.; Bally, M. B. Copper (II) complexes of bidentate ligands exhibit potent anti-cancer activity regardless of platinum sensitivity status. *Invest. New Drugs* **2017**, *35*, 682−690.

(44) Cater, M. A.; Pearson, H. B.; Wolyniec, K.; Klaver, P.; Bilandzic, M.; Paterson, B. M.; Bush, A. I.; Humbert, P. O.; La Fontaine, S.; Donnelly, P. S.; Haupt, Y. Increasing intracellular

bioavailable copper selectively targets prostate cancer cells. *ACS Chem. Biol.* **2013**, *8*, 1621−1631.

(45) Ray, S.; Mohan, R.; Singh, J. K.; Samantaray, M. K.; Shaikh, M. M.; Panda, D.; Ghosh, P. Anticancer and Antimicrobial Metal-lopharmaceutical Agents Based on Palladium, Gold, and Silver N-Heterocyclic Carbene Complexes. *J. Am. Chem. Soc.* **2007**, *129*, 15042−15053.

(46) Rai, A.; Kapoor, S.; Naaz, A.; Santra, M. K.; Panda, D. Enhanced stability of microtubules contributes in the development of colchicine resistance in MCF-7 cells. *Biochem. Pharmacol.* **2017**, *132*, 38−47.

(47) Tu, Q.; Wang, T.; Welch, C. J.; Wang, P.; Jia, X.; Raab, C.; Bu, X.; Bykowski, D.; Hohenstaufen, B.; Doyle, M. P. Identification and Characterization of Isomeric Intermediates in a Catalyst Formation Reaction by Means of Speciation Analysis Using HPLC−ICPMS and HPLC−ESI-MS. *Anal. Chem.* **2006**, *78*, 1282−1289.

(48) Martínez-Castro, E.; González-Benjumea, A.; López, Ó.; Maya, I.; Álvarez, E.; Fernández-Bolaños, J. G. Intramolecular cyclization of alkoxyaminosugars: access to novel glycosidase inhibitor families. *Org. Biomol. Chem.* **2012**, *10*, 4220−4228.

(49) Allen, F. H.; Johnson, O.; Shields, G. P.; Smith, B. R.; Towler, M. CIF applications. XV.enCIFer: a program for viewing, editing and visualizing CIFs. *J. Appl. Crystallogr.* **2004**, *37*, 335−338.

(50) Sheldrick, G. M. Crystal structure refinement withSHELXL. *Acta Crystallogr., Sect. C: Struct. Chem.* **2015**, *71*, 3−8.

(51) Dolomanov, O. V.; Bourhis, L. J.; Gildea, R. J.; Howard, J. A. K.; Puschmann, H. OLEX2: a complete structure solution, refinement and analysis program. *J. Appl. Crystallogr.* **2009**, *42*, 339−341.

(52) Chaudhary, V.; Venghateri, J. B.; Dhaked, H. P. S.; Bhoyar, A. S.; Guchhait, S. K.; Panda, D. Novel combretastatin-2-aminoimidazole analogues as potent tubulin assembly inhibitors: exploration of unique pharmacophoric impact of bridging skeleton and aryl moiety. *J. Med. Chem.* **2016**, *59*, 3439−3451.

(53) Asthana, J.; Kapoor, S.; Mohan, R.; Panda, D. Inhibition of HDAC6 deacetylase activity increases its binding with microtubules and suppresses microtubule dynamic instability in MCF-7 cells. *J. Biol. Chem.* **2013**, *288*, 22516−22526.

(54) Kumari, A.; Panda, D. Monitoring the disruptive effects of tubulin-binding agents on cellular microtubules.*Microtubules. Methods in Molecular Biology*; Inaba, H., Ed.; Humana: New York, NY, 2022; Vol. *2430*, pp 431−448.

(55) Panda, D.; Rathinasamy, K.; Santra, M. K.; Wilson, L. Kinetic suppression of microtubule dynamic instability by griseofulvin: implications for its possible use in the treatment of cancer. *Proc. Natl. Acad. Sci. U.S.A.* **2005**, *102*, 9878−9883.

(56) Hamel, E.; Lin, C. M. Glutamate-induced polymerization of tubulin: characteristics of the reaction and application to the large-scale purification of tubulin. *Arch. Biochem. Biophys.* **1981**, *209*, 29−40.

(57) Eberhardt, J.; Santos-Martins, D.; Tillack, A. F.; Forli, S. AutoDock Vina 1.2.0: New docking methods, expanded force field, and python bindings. *J. Chem. Inf. Model.* **2021**, *61*, 3891−3898.

(58) Schüttelkopf, A. W.; van Aalten, D. M. F. PRODRG: A tool for high-throughput crystallography of protein-ligand complexes. *Acta Crystallogr., Sect. D: Biol. Crystallogr.* **2004**, *60*, 1355−1363.

(59) Morris, G. M.; Huey, R.; Lindstrom, W.; Sanner, M.; Belew, R.; Goodsell, D.; Olson, A. J. AutoDock4 and AutoDockTools4: Automated docking with selective receptor flexibility. *J. Comput. Chem.* **2009**, *30*, 2785−2791.

(60) DeLano, W. L. *The PyMOL molecular graphics system.* http://www.pymol.org, 2002.

(61) Pettersen, E. F.; Goddard, T. D.; Huang, C. C.; Couch, G. S.; Greenblatt, D. M.; Meng, E. C.; Ferrin, T. E. UCSF Chimera-A visualization system for exploratory research and analysis. *J. Comput. Chem.* **2004**, *25*, 1605−1612.

(62) Kumari, A.; Panda, D. Investigating Tubulin-Drug Interaction Using Fluorescence Spectroscopy. *Microtubules. Methods in Molecular Biology*; Inaba, H., Ed.; Humana: New York, NY, 2022; Vol. *2430*, pp 261−276.